

Large Resonant Stokes Shift in CdS Nanocrystals

Zhonghua Yu,[†] Jingbo Li,[‡] Donald B. O'Connor,[†] Lin-Wang Wang,[‡] and Paul F. Barbara^{*,†}

Department of Chemistry and Biochemistry, Center for Nano- and Molecular Science and Technology, The University of Texas, Austin, Texas 78712, and NERSC, Lawrence Berkeley National Laboratory, Berkeley, California 94720

Received: November 5, 2002; In Final Form: April 23, 2003

The electronic spectrum of CdS colloidal quantum dots (QDs) with a radius of 1.0–2.3 nm is studied by low-temperature photoluminescence excitation spectroscopy. CdS QDs are found to exhibit a resonant Stokes shift of ~20–70 meV, which is ~4 times larger than similarly sized CdSe QDs. This effect can be reproduced by an effective-mass theoretical calculation, which reveals that the hole ground state (or highest occupied molecular orbital, HOMO) in CdS QDs is a P state and the ground-state exciton is an optically passive state. Compared to CdSe, in CdS, the smaller spin–orbit splitting causes the orbital-symmetry-forbidden dark exciton in a QD and its larger resonant Stokes shift. The band-edge photoluminescence in CdS QDs exhibits a lifetime of ~200 ns at 10 K, which is consistent with the dark exciton mechanism.

Introduction

Semiconductor nanocrystals (or quantum dots, QDs) represent a general class of materials that are intermediate between bulk materials and molecular species. Because of the quantum confinement effect, semiconductor nanocrystals exhibit size-dependent, molecular-like discrete electronic and optical transitions.^{1,2} There has been considerable research in this field, especially the optical properties of semiconductor QDs.³ Because of their unique electronic and optical properties, semiconductor QDs may find wide applications in future optoelectronics.

Among various semiconductors, CdSe QDs have been extensively investigated and have become a model system for understanding direct-band-gap semiconductor QDs, in part because the synthesis of high-quality, bright, and monodispersed CdSe QDs has been well developed.⁴ For example, high-quality CdSe QDs overcoated by ZnS or CdS show a band-edge emission quantum yield that is comparable to that of dye molecules.^{5,6} However, the band-edge emission mechanism is not fully understood. It was observed that the band-edge emission in CdSe QDs exhibited an unusually long decay lifetime (~1 μ s) at 10 K,^{7,8} in contrast to the nanosecond-scale lifetime in bulk CdSe. Also, the band-edge luminescence of a CdSe QD ensemble sample displays a nonresonant Stokes shift (the energy difference between the band-edge peak in absorption spectrum and the band-edge peak in emission spectrum) on the order of 50 meV, which is much larger than the resonant Stokes shift (the energy difference between the lowest-energy absorbing state and the emitting state) of constituent QDs photoselected by photoluminescence excitation (PLE) and fluorescence line narrowing (FLN) spectra.⁹ A surface state model was used to interpret the experimental observations in the early studies.⁷ Recently, a new model that is based on the fine structures of the internal semiconductor exciton state has been proposed for the band-edge emission process.¹⁰ In this mechanism, the

hexagonal crystal structure of the CdSe semiconductor, the nonspherical shape of CdSe nanocrystals, and the electron–hole exchange interaction lift the degeneracy of band-edge exciton states, which were previously considered to be highly degenerate. The ground state of the exciton is an optically passive or spin-forbidden dark state. After excitation, the CdSe QDs undergo rapid relaxation from upper absorbing states to the dark state, which can account for both the long emission-decay lifetime and the size-dependent resonant Stokes shift observed in CdSe QDs. A similar model has been applied previously to amorphous silicon,¹¹ which is an indirect-band-gap semiconductor.

CdSe QDs with different surface capping modifications have been studied, to examine the validity of the proposed models for the emission process.⁹ The lack of dependency of the optical properties on CdSe QD surface modification was consistent with the dark exciton model.

In the present study, we investigate the optical properties of band-edge emission from nanocrystals of a different semiconductor, CdS. Both CdS and CdSe have similar energy band structures, as shown schematically in Figure 1. However, they differ in carrier effective masses, crystal field splitting, and especially spin–orbit splitting (A–C band spacing) (0.07 eV in CdS, compared to 0.42 eV in CdSe), which should result in different degrees of state interaction in the electronic structure and thus different energy-level spacings in QDs. Theoretical calculations have already predicted that CdS QDs have a larger resonant Stokes shift, compared to CdSe.¹² Although CdS QDs have been extensively studied,^{13–20} deep-trap emission dominated the photoluminescence (PL) and tunable sizes of monodispersed QDs were not achieved. Recently a new synthetic method for high-quality CdS QDs has been developed,²¹ which will allow for the investigation of size-dependent band-edge emission in CdS QDs. In this paper, we investigate the size-dependent PL and PLE spectroscopy of CdS QDs. Theoretical calculations are also conducted to interpret the observed optical transitions and large resonant Stokes shift on the order of 20–70 meV in CdS QDs. Our results are consistent with the dark

* Author to whom correspondence should be addressed. E-mail: p.barbara@mail.utexas.edu.

[†] The University of Texas.

[‡] Lawrence Berkeley National Laboratory.

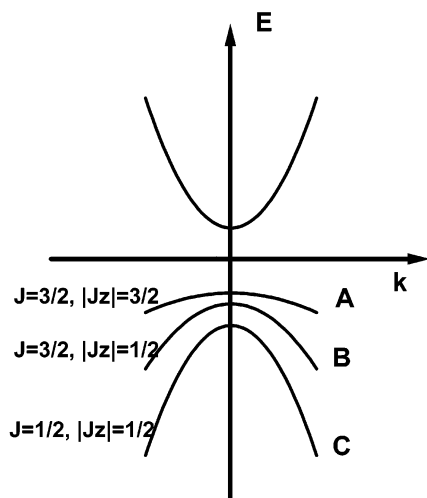


Figure 1. Schematic illustration of the bulk valence and conduction bands for wurtzite-type (hexagonal) semiconductors near $k = 0$. Because of the crystal field of the hexagonal lattice and spin-orbit coupling, the valence band is split into three bands (A, B, C). A–B and A–C are separated by crystal field splitting and spin-orbit splitting, respectively.

exciton model; however, the dark exciton is primarily associated with the orbital-symmetry-forbidden P-type hole ground state, because of the small spin-orbit splitting in CdS.

Experimental Section

CdS nanocrystals were synthesized according to a recently developed method.²¹ All the chemicals were purchased from Aldrich and used as received. The synthesis was conducted under an argon atmosphere. Typically, a 4-g mixture of CdO (0.0130 g), oleic acid (0.05–2.0 g), and octadecene (90%, technological grade) was heated in a 25-mL three-necked flask to 300 °C. The heat was then removed and the quick injection of a stock solution of 0.0016 g sulfur in 2-g of octadecene followed immediately, which cools the reaction mixture to ~ 250 °C. The heat was restored to allow the growth of CdS nanocrystals. The high concentration of oleic acid resulted in relatively large particles; in this case, the growth rate is so fast that no further heating is necessary after injection. These oleic acid-capped CdS particles were separated from octadecene by precipitation and centrifugation, using hexane/ethanol as a solvent/nonsolvent pair. The resulting powder of CdS nanocrystals is soluble in common organic solvents, such as chloroform, hexane, and pentane.

PL and PLE properties were measured with a Fluorolog II fluorimeter (Spex) in right-angle geometry. The room-temperature fluorescence quantum yield (QY) of CdS colloid solution was measured, relative to quinine sulfate in 0.1 N H_2SO_4 with 350-nm excitation (quinine sulfate QY of 51%).²² For low-temperature optical measurements, the CdS nanocrystals solution in a solvent mixture of methyl cyclohexane and *n*-pentane (volume ratio of 7:3) was sealed between two sapphire flats that were separated by a 1.5-mm-thick Teflon O-ring and mounted in a helium cryostat (ST-100, Janis). To avoid excitation scattering, the luminescence was collected from the back of the sample and at a right angle, relative to the excitation direction.

Fluorescence decay curves at variable temperatures were recorded by time-correlated single photon counting (TCSPC) with 350-nm vertically polarized excitation pulses ($\Delta t \approx 200$ fs, repetition rate of 1 MHz) from a mode-locked Ti:sapphire

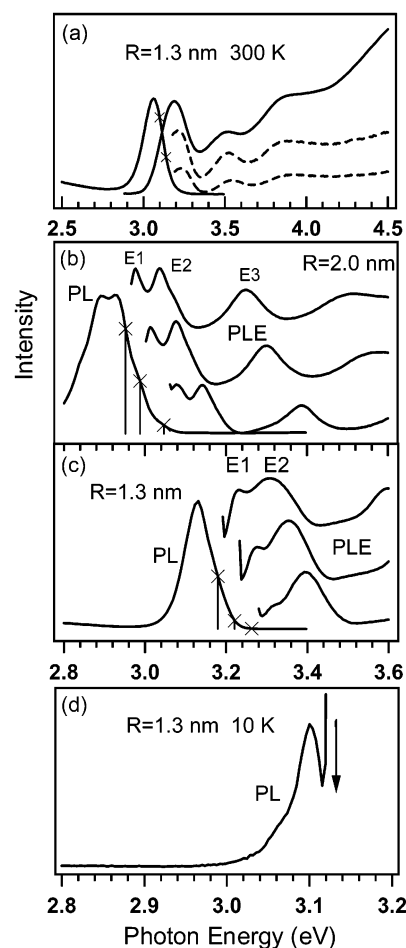


Figure 2. (a) Room-temperature absorption, emission, and excitation spectra of the 1.3-nm CdS quantum dots (QDs). (b, c) Low-temperature (10 K) emission and excitation spectra of the 1.3- and 2.0-nm CdS samples. In panels a–c, the cross sign (x) denotes the monitored fluorescence position for excitation spectra. The resolved absorption features are labeled by E1–E3. (d) Low-temperature (10 K) fluorescence line narrowing (FLN) spectrum of the 1.3-nm CdS sample; the downward arrow indicates the excitation photon energy.

laser system (Coherent Mira 900, Coherent pulse picker model 9200, Inrad SHG/THG model 5-050). Emission was detected at 90°, relative to the excitation axis with a microchannel plate detector (Hamamatsu model R3809U-50) through a band-pass filter (full width at half-maximum, fwhm, of 15 nm) and a Glan–Taylor polarizer (Karl Lambrecht) set at the “magic angle”. All emission decays were fit using an iterative nonlinear least-squares fitting procedure in which decay data was fit to a sum of exponential decays convoluted with the instrument response function (fwhm ≈ 50 ps).

Results

The new synthesis can make size-tunable, monodispersed wurtzite-type CdS nanocrystals that are capped by oleic acid ligands. Figure 2a shows the absorption, emission, and excitation spectra of the $R = 1.3$ nm (hereafter, all sizes are given in terms of radius) sample at room temperature. The average particle size was estimated from the first excitonic absorption peak position, on the basis of previous work.²¹ A few absorption features are clearly resolved in the spectra. The luminescence is dominated by the band-edge emission, except for the smallest particles. The nonresonant Stokes shift is ~ 125 meV for this sample at 300 K. The inhomogeneous line width of the emission is typically ~ 140 meV at 300 K. The room-temperature

luminescence QY of the 1.3-nm sample is 11% for band-edge emission and 12% for deep-trap emission. The QY of the 2.0-nm CdS sample band-edge and deep-trap emission are 15% and 4%, respectively.

The band-edge emission exhibits a monotonic blue-shift and simultaneous line narrowing as the temperature decreases. At 10 K, the blue-shift is as large as 70 meV, and the line width of the band-edge emission is only ~ 80 meV. The QY increases as the temperature decreases. At 10 K, the total QY is estimated to approach 100%, with the QY of band-edge emission being $\sim 50\%$. Both band-edge and deep-trap emissions gain intensity at low temperature; the band-edge emission does not gain intensity at the expense of the deep-trap emission. Thus, it is unlikely that the deep-trap emission is fed by the band-edge emission.

The PL and PLE spectra for two CdS samples ($R = 2.0$ and 1.3 nm) measured at 10 K are displayed in Figure 2b and c. The relatively broader PL line width in the 2.0-nm sample (~ 140 meV) is due to the broad size distribution resulting from the precipitation process. For PLE, the emission was monitored at the blue edge of the emission peak, to enhance spectroscopic resolution.²³ In low-temperature PLE spectra, up to eight features are resolved. Only the first few features (E1–E3) are shown, to focus on the resonant Stokes shift. The doublet structure (E1 and E2) with an energy spacing of ~ 0.07 eV, which is obscured in room-temperature PLE spectra, is now clearly resolved at low temperature. Similar doublet features were observed previously in hole-burning spectroscopy of CdS nanocrystals²⁴ and PLE spectra of larger CdS nanocrystals.²⁵ As in the CdSe system,²⁶ the spectral features are much narrower for larger-sized particles. Fluorescence line narrowing (FLN) spectrum for the 1.3-nm sample at 10 K is shown in Figure 2d, with the excitation energy located at the ensemble emission peak. The phonon structure is slightly resolved in this case.

The resonant Stokes shift in PLE spectroscopy is defined as the energy difference between the first absorbing peak E1 in PLE and the monitored emission energy. The obtained resonant Stokes shifts are plotted versus emission energy in Figure 3a for the 1.0-, 1.1-, 1.3-, and 2.0-nm samples. (The emission energy is used instead of QD size as the x -axis.²⁶ In PLE, the detection wavelength photoselects a narrow and more homogeneous distribution of QDs, relative to the ensemble distribution. The actual QD sizes are not well-known.) In FLN, the resonant Stokes shift, which also is plotted in Figure 3a, is the energy difference between excitation and the zero phonon line in emission. The values for the resonant Stokes shift obtained from FLN are consistent with PLE, as shown in Figure 3a. The resonant Stokes shift is in the range of ~ 20 – 70 meV for the samples investigated ($R \approx 1.0$ – 2.3 nm) and decreases with particle size. Note that the nonresonant Stokes shift (Figure 2a) is much larger than the resonant Stokes shift (Figure 2c). This is because, in the low-temperature PLE spectra of Figure 2b and c, we have resolved two fine peaks: E1 and E2. In size-averaged room-temperature absorption spectrum, these E1 and E2 peaks have merged into one peak with a center energy that is higher than that of the E1 peak. This results in a larger nonresonant Stokes shift. The second peak in the absorption spectrum of Figure 2a corresponds to the E3 peak in the low-temperature PLE spectra.

The PL decay lifetimes of the 1.1-nm sample were measured from 10 K to 298 K. Figure 4 shows the PL decay curves at 10 and 75 K, respectively, which reveals two principal decay components on sub-nanosecond and sub-microsecond scales. The slow component approaches a monoexponential decay at

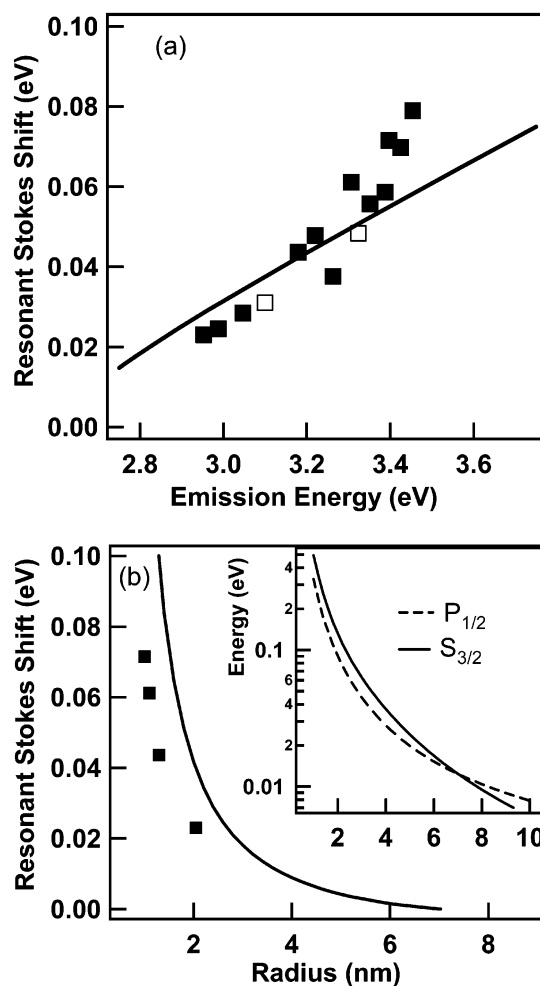


Figure 3. (a) Experimental resonant Stokes shift from (■) PLE and (□) FLN versus fluorescence energy. The theoretically predicted Stokes shift is also shown (as a solid curve). (b) Theoretically predicted (solid curve) and experimental (squares) resonant Stokes shift, as a function of the CdS QD radius. The inset in panel 3b shows the size dependence of $S_{3/2}$ and $P_{1/2}$ hole energy levels, where the subscripts 3/2 and 1/2 are the z -components of the angular momentum.

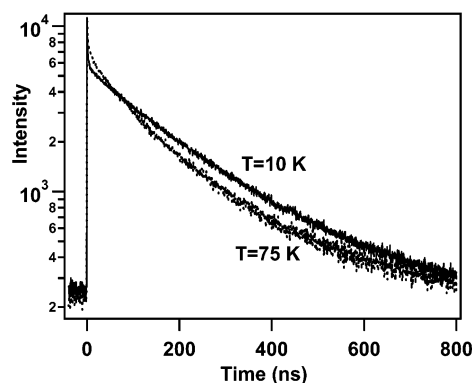


Figure 4. Semilogarithmic plot of photoluminescence decay curves of the 1.1-nm CdS sample at 10 and 75 K. The curves are characterized by a fast component (~ 1 ns) and a slow component (~ 200 ns).

10 K. It becomes a multiexponential decay as the temperature increases. The decay curves were fit with a single-exponential function for the fast component and a stretched exponential function for the slow component.^{27,28} The fast-component decay time is on the order of 1 ns. The slow-component decay time decreases from ~ 180 ns at 10 K to ~ 105 ns at 75 K, to ~ 40 ns at 150 K. It remains ~ 40 ns at room temperature.

Discussion

1. Resonant Stokes Shift. Our PLE and FLN results show that the resonant Stokes shift in the optical spectroscopy of CdS QDs are in the range of 20–70 meV, compared to 5–20 meV for similarly sized CdSe QDs.⁹ We conducted an effective-mass theoretical calculation on the exciton structures in these two systems and show here that the larger resonant Stokes shift in CdS QDs results from a different mechanism than that in CdSe QDs.

CdS and CdSe share the same lattice structure (wurtzite type). Thus, the bulk materials have very similar band structure, which is shown schematically in Figure 1. Here, J is the Bloch band-edge angular momentum ($1/2$ for the conduction band, $3/2$ for the heavy- and light-hole bands, and $1/2$ for the split-off band). The electron and hole wave functions each can be described by the product of a unit-cell Bloch basis function and an envelope function. The hole total angular momentum is $F = L + J$, where L is the envelope angular momentum. In wurtzite-type semiconductors, only the z -component of the total angular momentum F is a good quantum number. An effective-mass Hamiltonian for wurtzite-type semiconductors has been developed previously.²⁹ We calculate the electron and hole quantum-size levels in CdS QDs separately, without considering the coupling between the conduction and valence bands, because CdS is a wide-band-gap semiconductor ($E_g = 2.58$ eV at 0 K). The calculation is same as those in the work of Li and Xia.^{12,30} Briefly, the electron energy levels are given by

$$E_{l,n} = \frac{\hbar^2 (\alpha_{l,n})^2}{2m \left(\frac{R}{\epsilon_0}\right)^2}$$

where $\alpha_{l,n}$ is the n th zero point of the l th order spherical Bessel function $j_l(x)$. To calculate the hole energy levels, the effective-mass Hamiltonian for a wurtzite-type semiconductor was used,^{12,30} which considered the crystal field splitting and spin–orbit splitting explicitly. The parameters of electron and hole effective masses are adopted from refs 12 and 30. The crystal field splitting (0.024 eV) and spin–orbit splitting (0.07 eV) for CdS are from the work of Brus.³¹ We use nQ and nQ_m to represent the electron and hole states, respectively, where Q is the envelope angular momentum of the main component in the wave function and m is the z -component of the total angular momentum F .

As shown in the inset of Figure 3b, the calculation predicts that, in CdS QDs with a radius R less than ~ 7 nm, the ground-state hole level (or highest occupied molecular orbital, HOMO) is $1P_{1/2}$, whereas $1S_{3/2}$ is the HOMO in CdS QDs with $R > 7$ nm. This result agrees with the calculation by Efros and co-workers on a zincblende CdS lattice structure.^{32,33} Therefore, in CdS QDs with $R < 7$ nm, the exciton ground state is $1S_e1P_{1/2}$, rather than $1S_e1S_{3/2}$, as in CdSe QDs (where the subscripts $1/2$ and $3/2$ are the z -component angular momentums and $1S_e$ denotes the S envelope function of electron state). A P state is optically passive; therefore, the calculation suggests that the ground exciton in CdS QDs is an optically forbidden dark state. The first absorption state in CdS QDs is $1S_e1S_{3/2}$. After excitation to this absorption state, CdS QDs rapidly relax to the ground exciton state, which gives the band-edge emission. The energy difference between hole levels $1P_{1/2}$ and $1S_{3/2}$ then corresponds to the resonant Stokes shift in PL of CdS QDs. Figure 3b plots the calculated resonant Stokes shift for differently sized CdS QDs, in comparison with the experiment. Indeed, the calculated Stokes shift is in the same range as the experimental results, ~ 20 – 70 meV, although there is a systematic discrepancy between the calculation and the experiment.

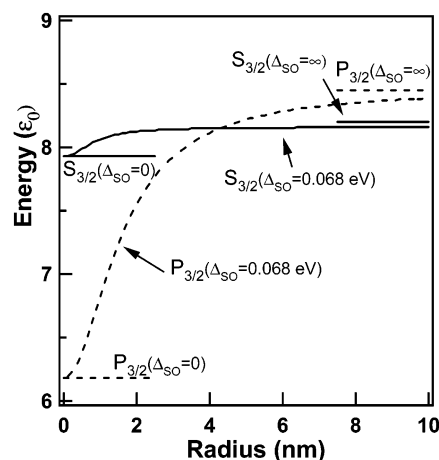


Figure 5. Spherical $k \cdot p$ model calculations of $1S_{3/2}$ and $1P_{3/2}$ states. Here, the subscript $3/2$ is the total angular momentum, which is a good quantum number in a spherical $k \cdot p$ model. Note that the spherical $k \cdot p$ model is further approximated from the $k \cdot p$ model that we used to calculate the results in Figure 3. The energy is given as $\epsilon_0 = \gamma_1/(2R)^2$, where the $k \cdot p$ parameters γ_1 and γ_2 are 0.98 and 0.34, respectively.

In Figure 3a, both calculated and experimental resonant Stokes shifts are plotted versus the emission energy. The PL emission energy is calculated as³⁴

$$E_{PL}(R) = E_g + E_{e,1S}(R) + E_{h,1P}(R) - \frac{1.8e^2}{\epsilon R}$$

where R is the QD radius and E_g is the band gap of CdS (2.58 eV). $E_{e,1S}$ ($E_{h,1P}$) is the energy of the electron (hole) quantum-size level $1S$ ($1P$). The last term accounts for the electron–hole coulombic interaction,³¹ where ϵ is the dielectric constant (5.7 for CdS). It can be seen that the theory quantitatively reproduces the experimental results very well. The deviation at high emission energy could be due to an overestimation of the band-edge transition for small QDs in the calculation.^{12,35}

The nature of the dark exciton is different in CdS and CdSe QDs. In CdSe QDs, the dark exciton is mainly due to exchange interaction and it is spin forbidden, whereas in CdS QDs, the dark exciton is mainly associated with a forbidden hole ground state (HOMO). The resonant Stokes shift resulting from electron–hole exchange interaction is on the order of 10 meV, as in CdSe,⁹ InAs,³⁶ and CdTe QDs,³⁷ which is much smaller than the resonant Stokes shift observed here in CdS QDs. In the case of CdS, on top of the orbital-forbidden dark exciton, there could still be an exciton fine-structure exchange splitting causing a spin forbiddenness at the exciton ground state.

Whether the $1S$ state or the $1P$ state is the hole ground state in a QD is dependent on the hole effective masses, the spin–orbit splitting parameter Δ_{so} , and the QD radius R . In a spherical $k \cdot p$ model, for the limiting case of $\Delta_{so} = \infty$, the $1S$ state is always the hole ground state (HOMO). If $\Delta_{so} = 0$, there are two hole effective masses: one for the heavy hole, and the other for the light hole. If the light-hole/heavy-hole effective-mass ratio is > 0.215 , the $1S$ state is the hole ground state; otherwise, the $1P$ state is the hole ground state. This is because, although the $1P$ state can be constructed entirely from the heavy holes, the $1S$ state has some components of the light hole. In the cases of CdS and CdSe, the $1P$ state is the hole ground state if $\Delta_{so} = 0$. Note that, for both $\Delta_{so} = \infty$ and 0 , the $1S$ and $1P$ state energies scale as $1/R^2$. Thus, using $1/R^2$ as the energy unit, the plots of the $1S$ and $1P$ state energies versus R are horizontal lines, as shown in Figure 5. In the case of finite Δ_{so} , for small R , when the confinement energy (which scales approximately as $1/R^2$)

is much larger than Δ_{so} , the situation is just like the case of $\Delta_{\text{so}} = 0$. On the other hand, for large R , when the confinement energy is much smaller than Δ_{so} , the situation is just like $\Delta_{\text{so}} = \infty$. This is illustrated in Figure 5, using a spherical $k \cdot p$ calculation. The 1S and 1P crossing point is located at the size where the confinement energy is approximately the same as Δ_{so} . Thus, for larger Δ_{so} (e.g., CdSe), the crossing point R will be smaller, which explains why, in the experimental range of R , the 1P state is the hole ground state for CdS but not for CdSe. Our combined experimental and theoretical studies of the resonant Stokes shift of CdS QDs provide strong evidence for the dark exciton mechanism that is associated with the symmetry-forbidden P-state HOMO.

2. Photoluminescence Lifetime at Low Temperature. The PL decay curve is also consistent with the dark exciton model in CdS QDs. In our experiment, the emission was selected by a 15-nm band-pass filter, so emission from both the dark state and the first absorbing state is detected. Because of the large Stokes shift in CdS, the emission is mainly from the dark state, with very little contribution from the absorbing state. Thus, the slow component is due to the dark-state decay. According to the same kinetic model as that proposed in the case of CdSe QDs,⁷ the fast component is due to the absorbing state, and its time constant is mainly determined by the relaxation rate from this state to the dark state. In CdSe, the PL decay curve was observed to change significantly with temperature,^{7,8} because of the equilibrium between the absorbing state and the dark state with a small energy gap (resonant Stokes shift). However, because of the large resonant Stokes shift in CdS, the PL decay curve only changes slightly when the temperature is increased from 10 K to 50 K. Thus, the dark exciton model can account for the PL decay at low temperature in CdS with a large resonant Stokes shift.

Summary

We investigated, both experimentally and theoretically, the large resonant Stokes shift that is exhibited by CdS quantum dots (QDs). Oleic acid-capped CdS QDs were synthesized to exhibit intense band-edge emission in UV and blue regions. Their electronic spectra were investigated by photoluminescence excitation, which reveals up to eight absorption features. CdS QDs are found to exhibit a resonant Stokes shift of ~ 20 – 70 meV, which is significantly larger than that of CdSe QDs of similar size. This large resonant Stokes shift is proposed, from the effective-mass calculation, to arise from an orbital-symmetry-forbidden dark exciton, in which the highest occupied molecular orbital (HOMO) is a P state. The origin of this dark exciton is different from that proposed for CdSe QDs. The formation of this type of forbidden state in CdS QDs is mainly due to the small spin–orbit splitting parameter Δ_{so} in CdS, which causes strong interaction between the valence bands. The low-temperature CdS QDs photoluminescence decay kinetics are consistent with the dark exciton model. The larger resonant Stokes shift exhibited in CdS QDs may render this type of material promising in optical applications such as light-emitting diodes and quantum dot lasers.

Acknowledgment. We thank Dr. William Yu and Dr. Xiaogang Peng for sending us a preprint of ref 21 before

publication and for the help in synthesizing CdS quantum dots. P.F.B. thanks the National Science Foundation and the Robert A. Welch Foundation for funding. J.L. and L.W.W. thank the U.S. Department of Energy for financial support. This work was funded in part by the U.S. Department of Energy, under Contract No. DE-AC03-76SF00098 (L.W.W.).

References and Notes

- (1) Alivisatos, A. P. *Science* **1996**, 271, 933.
- (2) Nirmal, M.; Brus, L. *Acc. Chem. Res.* **1999**, 32, 407.
- (3) Norris, D. J.; Bawendi, M. G.; Brus, L. E. Optical Properties of Semiconductor Nanocrystals (Quantum Dots). In *Molecular Electronics*; Jortner, J., Ratner, M., Eds.; Blackwell: Oxford, U.K., 1997; p 281.
- (4) Murray, C. B.; Norris, D. J.; Bawendi, M. G. *J. Am. Chem. Soc.* **1993**, 115, 8706.
- (5) Dabbousi, B. O.; Rodriguez-Viejo, J.; Mikulec, F. V.; Heine, J. R.; Mattoussi, H.; Ober, R.; Jensen, K. F.; Bawendi, M. G. *J. Phys. Chem. B* **1997**, 101, 9463.
- (6) Peng, X.; Schlamp, M. C.; Kadavanich, A. V.; Alivisatos, A. P. *J. Am. Chem. Soc.* **1997**, 119, 7019.
- (7) Bawendi, M. G.; Carroll, P. J.; Wilson, W. L.; Brus, L. E. *J. Chem. Phys.* **1992**, 96, 946.
- (8) Nirmal, M.; Murray, C. B.; Bawendi, M. G. *Phys. Rev. B* **1994**, 50, 2293.
- (9) Kuno, M.; Lee, J. K.; Dabbousi, B. O.; Mikulec, F. V.; Bawendi, M. G. *J. Chem. Phys.* **1997**, 106, 9869.
- (10) Nirmal, M.; Norris, D. J.; Kuno, M.; Bawendi, M. G.; Efros, A. L.; Rosen, M. *Phys. Rev. Lett.* **1995**, 75, 3728.
- (11) Calcott, P. D. J.; Nash, K. J.; Canham, L. T.; Kane, M. J.; Brumhead, D. J. *Phys.: Condens. Matter* **1993**, 5, L91.
- (12) Li, J.; Xia, J.-B. *Phys. Rev. B* **2000**, 62, 12613.
- (13) Chestnoy, N.; Harris, T. D.; Hull, R.; Brus, L. E. *J. Phys. Chem.* **1986**, 90, 3393.
- (14) Spanhel, L.; Haase, M.; Weller, H.; Henglein, A. *J. Am. Chem. Soc.* **1987**, 109, 5649.
- (15) Wang, Y.; Herron, N. *J. Phys. Chem.* **1988**, 92, 4988.
- (16) O'Neil, M.; Marohn, J.; McLendon, G. *J. Phys. Chem.* **1990**, 94, 4356.
- (17) Misawa, K.; Yao, H.; Hayashi, T.; Kobayashi, T. *J. Chem. Phys.* **1991**, 94, 4131.
- (18) Vossmeier, T.; Katsikas, L.; Giersig, M.; Popovic, I. G.; Diesner, K.; Chemseddine, A.; Eychmueller, A.; Weller, H. *J. Phys. Chem.* **1994**, 98, 7665.
- (19) Tittel, J.; Goehde, W.; Koberling, F.; Basche, T.; Kornowski, A.; Weller, H.; Eychmueller, A. *J. Phys. Chem. B* **1997**, 101, 3013.
- (20) Lakowicz, J. R.; Gryczynski, I.; Gryczynski, Z.; Murphy, C. J. *J. Phys. Chem. B* **1999**, 103, 7613.
- (21) Yu, W. W.; Peng, X. *Angew. Chem., Int. Ed.* **2002**, 41, 2368.
- (22) Velapoldi, R. A. *J. Res. Natl. Bur. Stand., Sect. A* **1972**, 76, 641.
- (23) Norris, D. J.; Efros, A. L.; Rosen, M.; Bawendi, M. G. *Phys. Rev. B* **1996**, 53, 16347.
- (24) Woggon, U.; Saleh, M.; Uhrig, A.; Portune, M.; Klingshirn, C. *J. Cryst. Growth* **1994**, 138, 988.
- (25) Chamarro, M.; Dib, M.; Voliotis, V.; Filoramo, A.; Roussignol, P.; Gacoin, T.; Boilot, J. P.; Delerue, C.; Allan, G.; Lannoo, M. *Phys. Rev. B* **1998**, 57, 3729.
- (26) Norris, D. J.; Bawendi, M. G. *Phys. Rev. B* **1996**, 53, 16338.
- (27) Soloviev, V. N.; Eichhofer, A.; Fenske, D.; Banin, U. *J. Am. Chem. Soc.* **2001**, 123, 2354.
- (28) Dag, I.; Lifshitz, E. *J. Phys. Chem.* **1996**, 100, 8962.
- (29) Xia, J.-B.; Li, J. *Phys. Rev. B* **1999**, 60, 11540.
- (30) Li, J.; Xia, J.-B. *Phys. Rev. B* **2000**, 61, 15880.
- (31) Brus, L. E. *J. Chem. Phys.* **1984**, 80, 4403.
- (32) Efros, A. L. *Superlattices Microstruct.* **1992**, 11, 167.
- (33) Efros, A. L.; Rosen, M. *Phys. Rev. B* **1998**, 58, 7120.
- (34) Efros, A. L.; Rosen, M. *Annu. Rev. Mater. Sci.* **2000**, 30, 475.
- (35) Banin, U.; Lee, C. J.; Guzelian, A. A.; Kadavanich, A. V.; Alivisatos, A. P.; Jaskolski, W.; Bryant, G. W.; Efros, A. L.; Rosen, M. *J. Chem. Phys.* **1998**, 109, 2306.
- (36) Banin, U.; Lee, J. C.; Guzelian, A. A.; Kadavanich, A. V.; Alivisatos, A. P. *Superlattices Microstruct.* **1997**, 22, 559.
- (37) Pérez-Conde, J.; Bhattacharjee, A. K.; Chamarro, M.; Lavallard, P.; Petrikov, V. D.; Lipovskii, A. A. *Phys. Rev. B* **2001**, 64, 113303.